


## METHOD REPORT

# A simple and highly efficient method for multi-allelic CRISPR-Cas9 editing in primary cell cultures

Pia Hoellerbauer<sup>1,2</sup> | Megan Kufeld<sup>1,3</sup> | Sonali Arora<sup>1</sup> | Hua-Jun Wu<sup>4</sup> |  
Heather M. Feldman<sup>1</sup> | Patrick J. Paddison<sup>1,2</sup> 

<sup>1</sup>Human Biology Division, Fred Hutchinson Cancer Research Center, Seattle, Washington

<sup>2</sup>Molecular and Cellular Biology Program, University of Washington, Seattle, Washington

<sup>3</sup>Antibody Discovery, Seattle Genetics, Bothell, Washington

<sup>4</sup>Department of Biostatistics and Computational Biology, Dana-Farber Cancer Institute, and Department of Biostatistics, Harvard School of Public Health, Boston, Massachusetts

## Correspondence

Pia Hoellerbauer, Fred Hutchinson Cancer Research Center, 1100 Fairview Ave N, C3-168, Seattle, WA 98109, USA.

Email: phoeller@fredhutch.org

Patrick J. Paddison, Fred Hutchinson Cancer Research Center, 1100 Fairview Ave N, C3-168, Seattle, WA 98109, USA.

Email: paddison@fredhutch.org

## Funding information

American Cancer Society, Grant/Award Number: ACS-RSG-14-056-01; National Institutes of Health, Grant/Award Numbers: P30 CA015704, P30 DK56465-13, R01 CA190957, T32 CA080416, U54 DK106829; Robert J. Kleberg, Jr. and Helen C. Kleberg Foundation

## Abstract

**Background:** CRISPR-Cas9-based technologies have revolutionized experimental manipulation of mammalian genomes. None-the-less, limitations of the delivery and efficacy of these technologies restrict their application in primary cells.

**Aims:** To create an optimized protocol for penetrant, reproducible, and fast targeted genome editing in cell cultures derived from primary cells, using patient-derived glioblastoma stem-like cells (GSCs) and human neural stem/progenitor cells (NSCs) for proof-of-concept experiments.

**Methods and results:** We employed transient nucleofection of Cas9:sgRNA ribonucleoprotein complexes composed of chemically synthesized 2'-O-methyl 3'phosphorothioate-modified sgRNAs and purified Cas9 protein. Insertion-deletion mutation (indel) frequency and size distribution were measured via computational deconvolution of Sanger sequencing trace data. We found that this optimized technique routinely allows for >90% indel formation in only 3 days, without the need to create clonal lines for simple loss-of-function experiments. Using Western blotting, we observed near-total protein loss of target genes in cell pools. Additionally, we found that this approach allows for the creation of targeted genomic deletions. Furthermore, by using RNA-seq in edited NSCs to assess gene expression changes resulting from knockout of tumor suppressors commonly altered in glioblastoma, we also demonstrated the utility of this method for quickly creating a series of gene knockouts that allow for the study of oncogenic activities.

**Conclusion:** Our data suggest that this relatively simple method can be used for highly efficient and fast gene knockout, as well as for targeted genomic deletions, even in hyperdiploid cells (such as GSCs). This represents an extremely useful tool for the cancer research community when wishing to inactivate not only coding genes, but also non-coding RNAs, UTRs, enhancers, and promoters. This method can be readily applied to diverse cell types by varying the nucleofection conditions.

## KEYWORDS

Cas9:sgRNA ribonucleoprotein, CRISPR-Cas9, gene editing, genomic deletion, glioblastoma stem-like cells, neural stem cells

This is an open access article under the terms of the Creative Commons Attribution NonCommercial License, which permits use, distribution and reproduction in any medium, provided the original work is properly cited and is not used for commercial purposes.

© 2020 The Authors. *Cancer Reports* published by Wiley Periodicals LLC.

## 1 | BACKGROUND

In bacteria and archaea, the CRISPR-Cas (Clustered, Regularly Interspaced, Short Palindromic Repeats [CRISPR]-CRISPR-associated [Cas]) pathway acts as an adaptive immune system, conferring resistance to genetic parasites and bacteriophage.<sup>1,2</sup> CRISPR-Cas systems are able to target and degrade DNA,<sup>1,2</sup> and this property has been harnessed for directed genome editing in prokaryotes and (more recently) eukaryotes, including human cells,<sup>3-6</sup> using the type II CRISPR-Cas system from *Streptococcus pyogenes*. In its simplest form, this system consists of a complex of two components, the Cas9 protein and a single guide RNA (sgRNA). Cas9 is an RNA-guided DNA endonuclease. The sgRNA is a chimeric guide RNA (gRNA) composed of a ~20 nt "protospacer" sequence, which is used for target recognition, and a structural RNA required for Cas9:sgRNA complex formation (ie, tracrRNA). In addition, DNA cleavage by Cas9 occurs only in the presence of an appropriate protospacer adjacent motif (PAM) at the 3' end of the protospacer sequence in the target genomic locus (for Cas9 this is "NGG," where N is any nucleotide<sup>2</sup>).

When Cas9 and an sgRNA are expressed together, a double-strand DNA (dsDNA) break is created about 3 bp upstream of the PAM site.<sup>7,8</sup> This break is then repaired by the cell either via the high-fidelity homology-directed repair (HDR) pathway, or much more commonly, via the error-prone non-homologous end joining (NHEJ) pathway, which leaves behind repair scars in the form of small insertion-deletion (indel) mutations.<sup>9,10</sup> When these indels occur in an exon, they can cause frameshifts and premature stop codons in the target gene, effectively ablating protein function.<sup>4,6,11</sup>

Cas9:sgRNA targeting efficiency in human cells varies considerably depending on the methods, reagents, and cell types used. In general, successful generation of indels using transient DNA transfection occurs in a range of ~1% to 30%.<sup>8</sup> However, it was shown that lentiviral-based stable expression of Cas9:sgRNA greatly improves targeting efficiency to >90%.<sup>2,12,13</sup> As a direct result, we and others have successfully performed pooled lentiviral-based sgRNA screens in various human cell types.<sup>12-14</sup> However, retesting single sgRNAs from these screens, especially those targeting essential genes, can prove challenging. For example, in human neural stem/progenitor cells (NSCs) and patient-derived glioblastoma stem-like cells (GSCs), we have observed that "all-in-one" lentiviral-based CRISPR systems can result in protracted windows of indel formation and phenotypically mixed populations, requiring incubation of up to 12 days to achieve complete indel formation.<sup>14</sup> As a result, it can be difficult to set up rigorous experiments analyzing a particular gene knockout (KO) when cell populations contain variable mixtures of wild-type (wt) and indel-containing alleles and, if the target gene is essential, thereby contain mixtures of alive and dead cells. This represents a critical experimental limitation of the use of CRISPR-Cas9 platforms in primary cells. As a result, we wished to create an optimized protocol that would allow for maximal targeted indel formation over the shortest possible experimental window.

We therefore explored alternative approaches, including the use of Cas9:gRNA ribonucleoprotein (RNP) complexes composed of purified Cas9 protein and purified gRNA. Compared to lentiviral and

DNA-based methods, direct delivery of CRISPR-Cas9 RNPs allows for increased control over the dosing and duration of exposure of cells to the CRISPR-Cas9 reagents. Since RNP methods do not rely on the cells themselves to generate Cas9 protein and gRNA, editing can happen much more rapidly. In addition, since RNPs are quickly naturally degraded by the cell and/or eliminated by dilution during mitosis, the opportunity for off-target editing is reduced compared to lentiviral and DNA-based methods, which typically result in sustained over-expression of CRISPR-Cas9 components.<sup>15</sup>

Cas9:gRNA RNPs have recently been used effectively for several applications, including gene loss-of-function in human cell lines<sup>16-18</sup> and ES cells,<sup>16</sup> editing of *CXCR4* in human T cells,<sup>19</sup> HDR tests in human cells via insertion of restriction sites,<sup>16,20</sup> epitope tagging in mouse NSCs,<sup>21</sup> and studying effects of sgRNA sequence on editing efficiency.<sup>22</sup> The efficiencies reported for in vitro editing in these contexts are most often in the range of ~15% to 60%, with most studies reporting *maximum* (not routine) efficiencies ≤80%. We wanted to further improve upon these RNP methods so we could routinely achieve high efficiency, multi-allelic editing in cell cultures derived from primary cells, such as GSCs and NSCs.

We found a robust method that utilizes transient nucleofection of in vitro-formed Cas9:sgRNA RNP complexes composed of chemically synthesized, 2'-O-methyl 3'phosphorothioate-modified sgRNAs and purified Cas9 protein. With this optimized approach, we are able to achieve >90% indel formation in multiple human GSCs and NSCs in only 3 days (overview in Figure 1A). Because indel frequencies are so high, mixed populations of cells can be used for simple loss-of-function experiments, eliminating the need to create clonal lines. In addition, we find that our approach allows for the creation of targeted deletions in cell pools (for smaller desired deletions, eg, ~50-1000 bp) or cell clones (for larger desired deletions, eg, ~50 kbp). Here we present these results illustrating the utility of this method and a detailed step-by-step protocol (Data S1).

## 2 | RESULTS

### 2.1 | Nucleofection of Cas9:sgRNA (chemically synthesized, 2'-O-methyl 3'phosphorothioate modified) RNPs results in highly penetrant and fast generation of small indels in human GSCs and NSCs

Since most studies using Cas9:gRNA RNPs utilize in vitro-transcribed gRNA, and we wanted to further improve upon the efficiencies reported in these studies, we instead tested chemically synthesized sgRNAs, with or without 2'-O-methyl 3'phosphorothioate modifications (in the first and last three nucleotides). These modifications protect sgRNAs from degradation by nucleases and therefore likely increase RNP half-life.<sup>23-26</sup> We formed RNPs by combining these sgRNAs with purified sNLS-SpCas9-sNLS nuclease and then delivered them via nucleofection, a modified electroporation technique (developed by Amaxa, now Lonza) that allows direct transfer of nucleic acids into the nuclei of mammalian cells in culture.

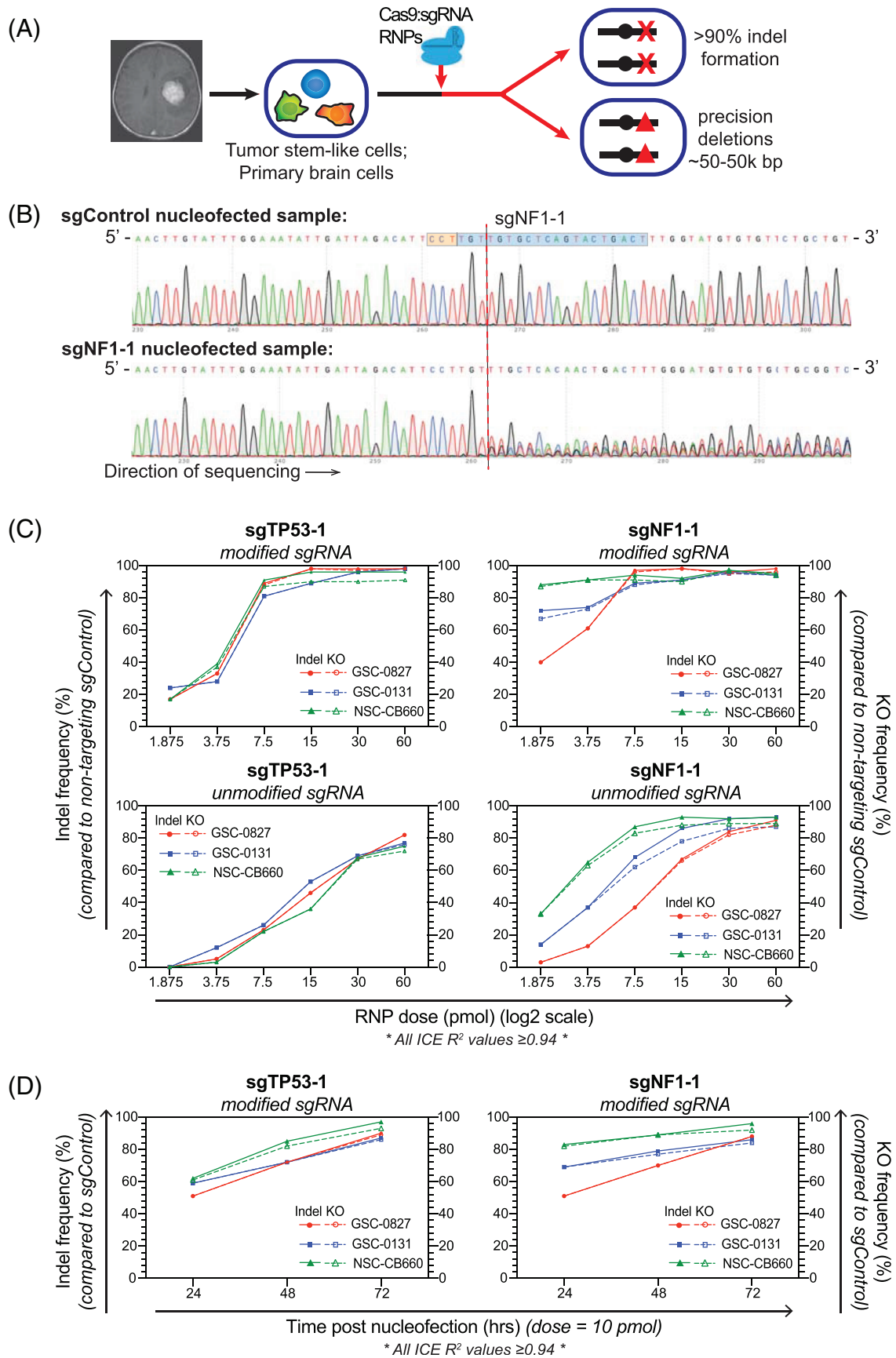


**FIGURE 1** Legend on next page.

To follow indel formation in cell pools, we employed a method that uses Sanger sequencing of sgRNA target site-spanning PCR amplicons followed by computational trace decomposition of the control and experimental traces to predict indel frequency.<sup>27,28</sup> This method relies on the fact that CRISPR-edited cells produce a clean sequencing trace that mirrors control cells up until the sgRNA cut site, at which point the trace for edited cells begins to represent the compounding effect of multiple overlapping traces due to various indel mutations (Figure 1B). A bioinformatics tool (Inference of CRISPR Edits, or "ICE")<sup>28</sup> can be used to generate a prediction for which overlapping DNA sequences explain the observed trace in the edited sample. This allows for a breakdown of indel sequence distribution and a measurement of % wt vs % indel sequences in the cell pool. Using this information, KO frequency can also be estimated by assessing the percent of predicted sequences that result in either a frameshift or a larger indel ( $\geq 21$  bp in length), since such cases are likely to result in a non-functional protein product.<sup>28</sup>

In order to determine the efficiency of indel formation using nucleofection of Cas9:sgRNA RNPs, we measured indel and KO frequency for doses ranging from  $\sim 2$  to 60 pmol in diploid NSC-CB660 cells, near-diploid GSC-0131 cells, and hypertriploid GSC-0827 cells, for single sgRNAs targeting *TP53* exon 7 (sgTP53-1) and *NF1* exon 2 (sgNF1-1) (Figure 1C). *TP53* and *NF1* are both located on chromosome 17, of which GSC-0131 have 2 copies and GSC-0827 have 3 copies. These experiments revealed that when using 2'-O-methyl 3'-phosphorothioate modified sgRNAs, high (>90%) multi-allelic indel efficiencies can be achieved starting at RNP doses of 7.5 to 15 pmol in GSCs and NSCs (Figure 1C, top panels). Unmodified sgRNAs provided inferior editing compared to modified sgRNAs, requiring higher doses of RNPs to achieve the same level of indel formation (Figure 1C, bottom panels). We therefore chose to use only modified sgRNAs for the remainder of our experiments.

In order to assess the timing of CRISPR editing using our system, we also measured indel and KO frequency at 24, 48, and 72 hours post-nucleofection for an RNP dose of 10 pmol (Figure 1D). We observed that  $\sim 50\%$  to 80% of editing has occurred by 24 hours post-nucleofection, reaching its maximum by 72 hours (Figure 1D). Similar indel penetrance for sgRNAs targeting other genes was also observed in multiple GSC isolates and in NSCs which had been immortalized and oncogenically transformed (Figure S1). Because many of our sgRNA sequences had been prevalidated through our

lentiviral screens<sup>14</sup> (eg, sgTP53-1; sgNF1-1; 13 of 23 sgRNAs in Figure S1), these experiments illustrate representative results for active RNPs. Of note, several of the genes targeted are present at hyperdiploid levels in GSCs; for instance, GSC-G166 contain 3 copies of *SCAP*, *FBXO42*, and *GMPPB*. Furthermore, targets included top scoring essential genes for both GSCs and NSCs, which cause profound viability loss,<sup>14</sup> indicating that the high efficiencies we observe are not simply due to outgrowth of edited cells.

High on-target CRISPR-Cas9 activity can sometimes come at the expense of high off-target activity.<sup>29</sup> Therefore, in order to gauge off-target activity using our system, we looked for CRISPR editing at the top six predicted off-target sites for the sgRNAs we had used for *TP53* and *NF1*. While we observed high on-target editing (98% indel formation for sgTP53-1 and 96% for sgNF1-1), we did not observe any indels at any of these off-target sites (Figure S2). This supports the notion that the transient delivery of Cas9:sgRNA RNPs can limit potential off-target effects, particularly if care is taken to design sgRNAs that take up-to-date off-target prediction criteria into account (see Methods).

## 2.2 | RNP nucleofection allows for targeted deletion of several hundred bp genomic regions

In our efforts to assess RNP efficiency and dosing, we also noted that when using single sgRNAs, the KO efficiency often closely mirrored the indel efficiency (Figure 1C,D). This is due to repair bias at the target sites, since we observed that individual sgRNAs often produced a high percentage of 1 bp insertions or deletions (Figure 2A,B, top and middle panels). This is consistent with a recent analysis of sgRNA targeting repair events in human cells, which found that frameshift frequencies are higher than expected (81% vs the expected 67% for random NHEJ-mediated repair), due to unexpectedly high 1 bp insertion/deletion events.<sup>11</sup>

Given the precise and reproducible nature of the indels created for single sgRNAs using our system, we wondered if using two sgRNAs in close proximity (eg, 50-1000 bp) would favor the production of precise deletions (that is, deletion of the entire region between the two sgRNA cut sites) rather than small indels. This was indeed the case when we simultaneously nucleofected with two sgRNAs targeting *TP53* or *NF1* (Figure 2A,B, bottom panels). We observed

**FIGURE 1** Highly efficient and fast indel formation using RNPs composed of purified Cas9 and chemically synthesized, 2'-O-methyl 3'-phosphorothioate-modified sgRNA. A, Overview of CRISPR RNP targeting strategy. B, Sanger sequencing trace example of the genomic region around the sgRNA cut site for a pool of NSC-CB660 nucleofected with 15 pmol RNPs using either a non-targeting control sgRNA or sgNF1-1 (72 hours post-nucleofection). Sequence was created using a reverse sequencing primer. Blue shaded box denotes sgRNA, orange shaded box denotes PAM sequence, and dotted red line represents sgRNA cut site. Sanger trace data like this was used in conjunction with a freely-available bioinformatics tool ("ICE") in order to predict CRISPR editing sequence distribution in cell pools. C, CRISPR editing efficiency as a function of RNP dose for two different sgRNAs that were either 2'-O-methyl 3'-phosphorothioate-modified (top panels) or unmodified (bottom panels). Solid data lines denote indel frequency while dotted lines denote predicted KO frequency (% of predicted sequences that result in a frameshift or an indel  $\geq 21$  bp in length). All samples were harvested 72 hours post-nucleofection. ICE  $R^2$  values represent "goodness of fit" for the bioinformatics model used to predict indel frequencies from Sanger trace data. D, CRISPR indel frequency and KO frequency as a function of time post-nucleofection for two different sgRNAs (2'-O-methyl 3'-phosphorothioate-modified). A dose of 10 pmol was used

high predicted exact deletion frequencies of 53-85% for GSCs and NSCs (Figure 2C). Allowing ±2 bp for the deletion size window further increased the predicted “near-precise” deletion efficiencies to a

remarkable 81-93% (Figure 2C). It is also important to note that in this multiple sgRNAs scenario, the bioinformatic predictions for total indel frequencies were at times somewhat reduced due to adjustment for

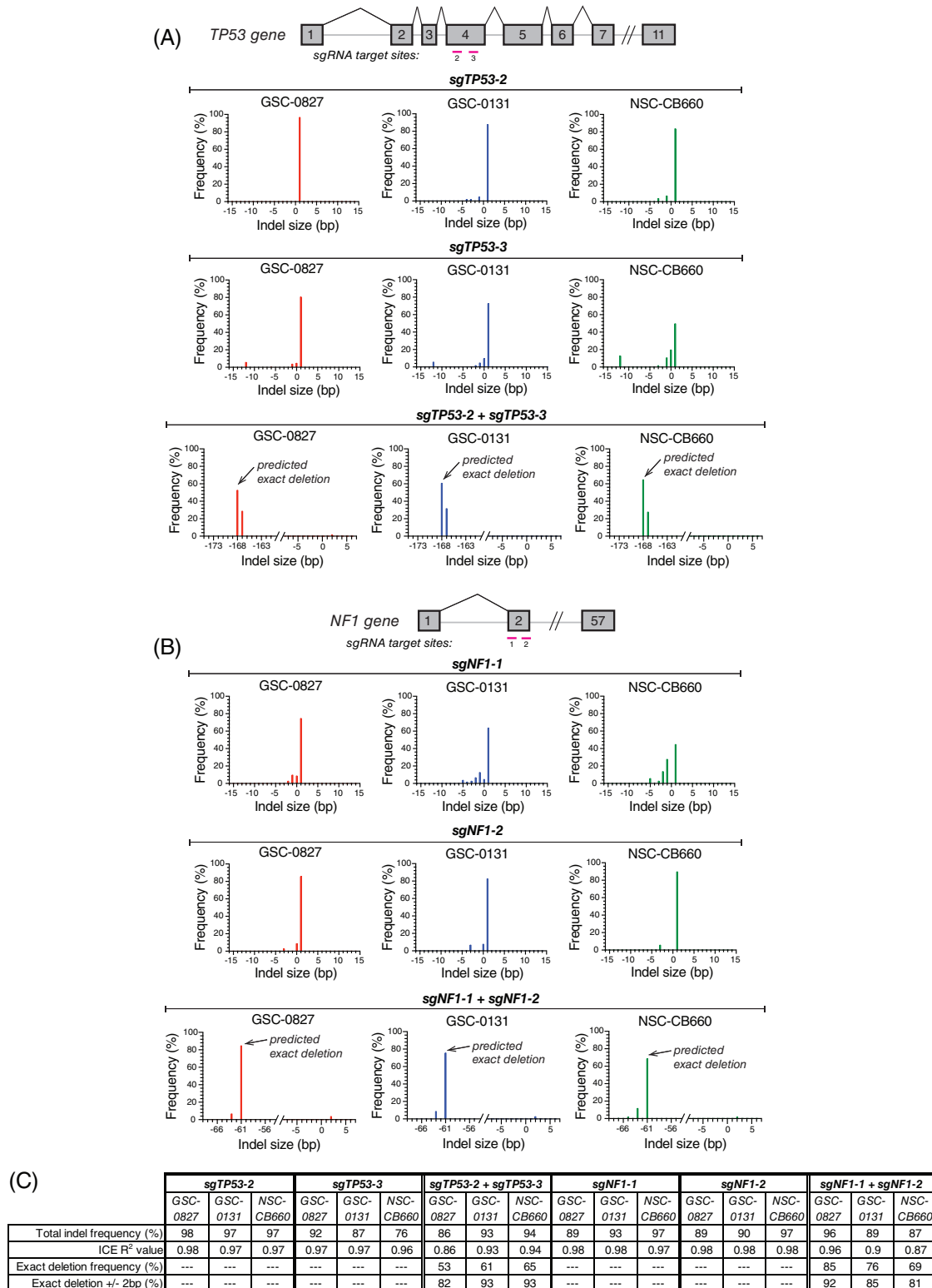


**FIGURE 2** Cas9:sgRNA RNPs can be used to create small targeted deletions. A, Indel size distribution of predicted indel sequences for cell isolates nucleofected with individual sgTP53s (top two panels) or two simultaneous sgTP53s (bottom panel) (168 bp apart). B, Indel size distribution of predicted indel sequences for cell isolates nucleofected with individual sgNF1s (top two panels) or two simultaneous sgNF1s (bottom panel) (61 bp apart). C, Summary of sgRNA indel profiles shown in A and B. ICE R<sup>2</sup> values represent “goodness of fit” for the bioinformatics model used to predict indel distributions from Sanger trace data

slightly lower regression fit  $R^2$  values. However, essentially 0% wt sequences were predicted in the trace data (see indel size of "O" in bottom panels of Figure 2A,B), suggesting that the total indel frequencies - and thereby also the deletion frequencies - may actually have been even higher. We observed similar near-precise deletion results when nucleofecting with two other sets of double sgRNAs (Figure S3).

To further investigate these results, we designed sets of 3 sgRNAs to target 13 different non-coding genomic loci on chromosomes X, 2, 5, 13, 15, and 21 in GSC-0827 cells, which contain 4, 3, 3, 2, 3, and 3 copies of these chromosomes, respectively. These sgRNA sequences were designed using the Broad GPP Web Portal<sup>30</sup> and were used without revalidation. Each target locus was defined by two outer/flanking sgRNA cut sites (176-981 bp apart) and a third sgRNA targeting roughly the midpoint (Figure S4A). Five days after nucleofection using these sgRNA pools (compared to a non-targeting control sgRNA), deletion production was visualized via PCR using primers flanking the outermost cut sites (Figure S4A). The results revealed that deletions, spanning either the flanking cut sites or a flank-to-mid cut, were dramatically favored over simple small indels (which are contained in the ~wt-sized band due to lack of separation for size differences of only a few bp) (Figure S4B). Taken together, our results suggest that near-precise deletions of lengths <1000 bp can be readily generated using this protocol.

### 2.3 | RNP nucleofection generates dramatic protein loss in cell pools

Given the potential of our approach to create highly penetrant multi-allelic KO in cell pools, we wanted to further demonstrate its utility by creating a series of KO mutants in human NSCs, which are a candidate cell-of-origin of GSCs<sup>31-37</sup> and can be used to model oncogenic transformation in glioblastoma. Previously, we and others have used ectopic expression of human oncogenes (eg, *EGFRvIII*, *RasV12*, *Myr-Akt1*, *CCND1*, *CDK4<sup>R24C</sup>*, dominant-negative *TP53*) to partially or completely transform NSCs.<sup>14</sup> Our current method afforded us the opportunity to affect the same pathways by instead creating loss-of-function mutations in tumor suppressors. We chose to successively target four genes commonly mutated or deleted in adult glioblastoma tumors: *TP53*, *CDKN2A*, *PTEN*, and *NF1*, which affect distinct pathways required for glioma progression, including the p53-pathway, the Rb-axis, the PI3-k/AKT pathway, and the RTK-Ras-MAPK pathway.<sup>38</sup>

We nucleofected TERT-immortalized NSC-CB660 cells with pools of 3 sgRNAs for each gene, in four successive rounds of nucleofection spaced 1 week apart (to allow cells time to recover from electroporation) (Figure 3A). In this case, we chose to spread the sgRNAs across each gene to favor individual indels rather than deletions, reasoning that the cumulative effect of 3 sgRNA sites for each gene would lead to a high percentage of cells that contained at least one out-of-frame edit in each allele. We examined the effect on target protein expression via Western blotting on the pool at each stage in the process, as well as on eight subclones of the final pool. Remarkably, we observed dramatic protein loss for each gene in the targeted pools (Figure 3B).

Examination of the eight clones of the final *TP53* + *CDKN2A* + *PTEN* + *NF1* targeted KO pool revealed a similar result, where all proteins showed similar reduction in individual clones, except for one clone which still showed protein expression of *NF1* (Figure 3C).

### 2.4 | RNP nucleofection allows for targeted biallelic deletion of multi-kb genomic regions

We also assessed indel efficiencies in the tumor suppressor KO cell pools across one test sgRNA for each gene. For *TP53*, *CDKN2A*, and *NF1* we observed high predicted indel frequencies of 98%, 95%, and 95%, respectively. For *PTEN*, however, we noted a discrepancy between the Western blot results, which showed near-total ablation of protein expression, and the indel analysis for all 3 sgRNAs, which each revealed only ~33% efficiency. Since probability suggests that even the cumulative editing effect of these 3 sgRNAs should not quite account for near-total protein loss, we suspected that the *PTEN* sgRNA pool may have allowed for the generation of a large deletion. To investigate this possibility, we performed PCR with primers flanking the outer sgRNA cut sites (Figure 4A). In this case, an allele that did not harbor deletion of the entire ~64 kbp region would not amplify properly in our PCR conditions since the product would be too large. We observed that 2 of 8 clones tested contained a deletion allele, and one of these actually produced two products of similar but distinct sizes, indicating a biallelic deletion with slightly different editing results (Figure 4B, left panel). As a positive control for gDNA integrity, we used a second PCR spanning a small *PTEN* region outside the deletion region, and we observed the correct product for all 8 clones in this case (Figure 4B, right panel).

Gel-purification of the deletion PCR bands followed by Sanger sequencing confirmed that each deletion allele observed in the clones was a result of cutting near the predicted outermost sgRNA cut sites, with one allele tested being an exact deletion, one containing an additional 1 bp insertion, and one containing an additional 10 bp 5'-deletion and 48 bp 3'-deletion (Figure 4C). To further investigate this, we performed RNA-seq and examined reads mapping to the *PTEN* locus in the KO pool and in clone 1. Analysis of predicted "splice junctions" based on RNA-seq reads showed that mRNA containing the exact deletions observed at the gDNA level could be identified in clone 1, and no properly spliced reads were present, corroborating the fact that this clone did not contain any non-deletion allele (Figure 4D). Furthermore, reads corresponding to large deletions could be observed in the cell pool as well, in addition to the expected normally spliced reads. These results suggest that using multiple sgRNAs with our method has the potential to create large (>50 kbp) deletions, which may be monoallelic or biallelic in subsets of clones.

### 2.5 | Analysis of gene expression changes induced by tumor suppressor KO targeting events

To further assess the fidelity of gene KOs via CRISPR RNP nucleofection, we examined the progressive changes in gene

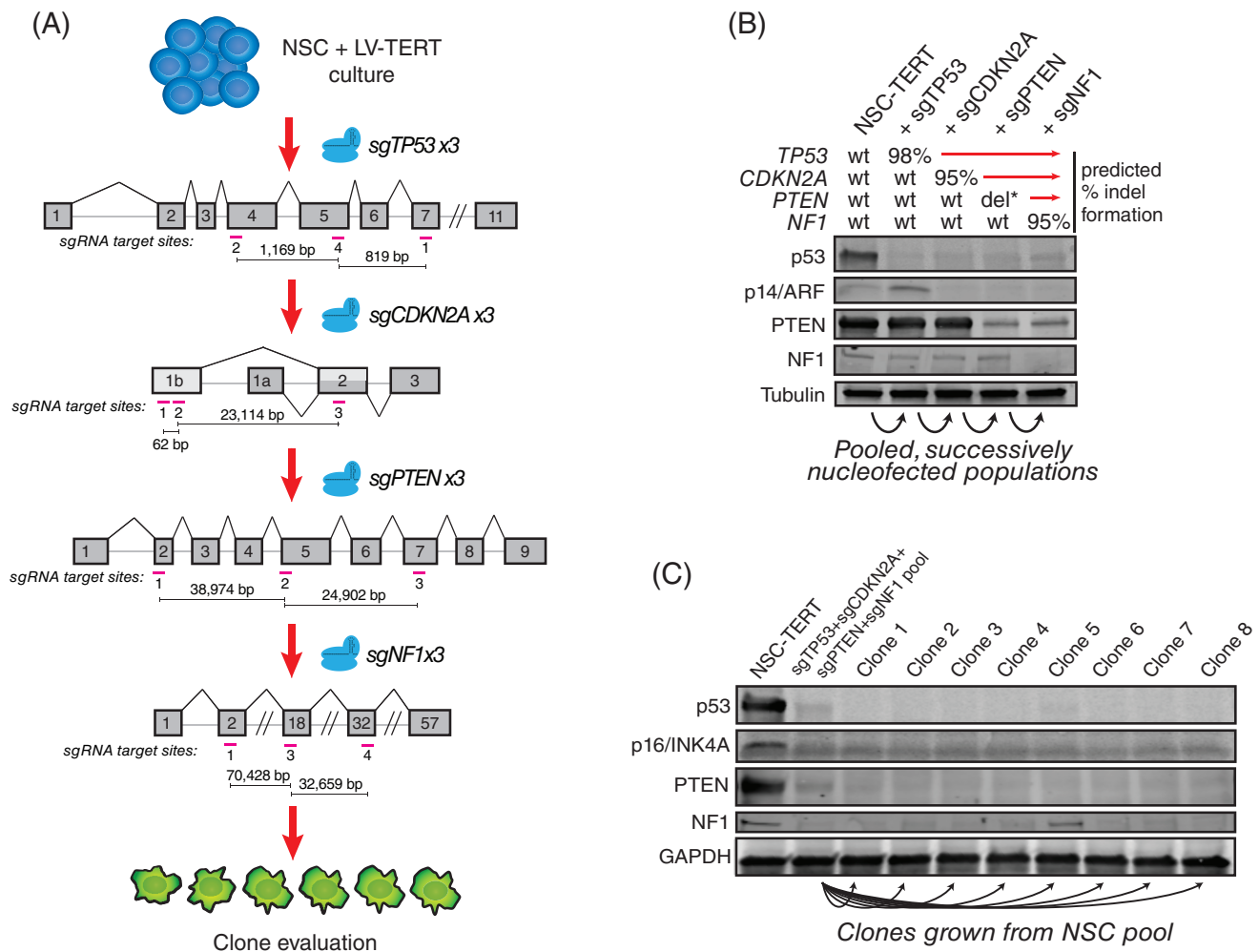


**FIGURE 3** Use of Cas9:sgRNA RNPs to generate multi-gene knockout cell pools to model oncogenic transformation reveals dramatic protein loss. A, Overview of strategy for successive Cas9:sgRNA RNP nucleofections targeting various tumor suppressors in NSCs. B, Western blots for targeted genes in the cell pool at each successive stage. Predicted % indel formation for representative sgRNA for each gene from Sanger sequencing results is shown above blot. Del\* indicates that large deletions were identified in addition to indels (detailed in Figure 4). For detection of p53, cells were treated with doxorubin to stabilize the protein. C, Western blots for 8 clones derived from the final NSC-TERT sgTP53 + sgCDKN2A + sgPTEN + sgNF1 cell pool

expression after each successive targeting event (sgTP53, sgCDKN2A, sgPTEN, sgNF1) in NSC-CB660-TERT cells, by performing RNA-seq on the parental cells compared to the targeted cells at each stage. We used edgeR<sup>39</sup> for differential gene expression analysis, and Figure 5A shows the overall relationship of these data in cluster analysis and the gene expression changes after each targeting. The greatest number of changes were produced by TP53 KO (269 genes with  $\log_2$  fold-change [ $\log_2FC$ ] > 0.5 and 682 genes with  $\log_2FC$  < -0.5 [FDR < 0.05]) and CDKN2A KO (1340 genes with  $\log_2FC$  > 0.5 and 1733 genes with  $\log_2FC$  < -0.5 [FDR < 0.05]). Importantly,  $\geq 80\%$  of TP53 KO-induced expression changes were maintained (at FDR < 0.05) even after further CDKN2A KO, PTEN KO, and NF1 KO, and  $\geq 78\%$  of CDKN2A KO-induced expression changes were maintained even after further PTEN KO and NF1 KO.

The gene expression changes associated with TP53 KO cells were consistent with p53's known transcriptional function. We observed downregulation of key p53 transcriptional targets, including 27 of 132 found in Pathway Interaction Database ( $P = 8.2E-20$ ) and 51 of 116 literature-curated p53 targets, including: BAX, BBC3/PUMA, BTG2, CDKN1A/p21, RRM2B, and ZMAT3<sup>40</sup> (Figure 5B,C; Tables S2 and S3). CDKN2A KO cells most prominently revealed upregulation of genes associated with the cell cycle (285 genes; GO:0007049;  $P = 6E-116$ ) and specifically E2F targets (52 genes;  $P = 2.4E-42$ ), including E2F1 and E2F2 themselves (Figure 5B,C; Tables S2 and S3). This is consistent with loss of CDKN2A's p16 protein, which inhibits Cyclin D/CDK activity in G1, preventing de-repression of E2F.<sup>41</sup> Other prominent cell cycle regulated genes included those associated with: CDK1 interactions (67 genes,  $P = 1.7E-28$ ), MCM6 interactions (33 genes,  $P = 6.1E-19$ ), PCNA interactions (64 genes,  $P = 6.2E-28$ ), and

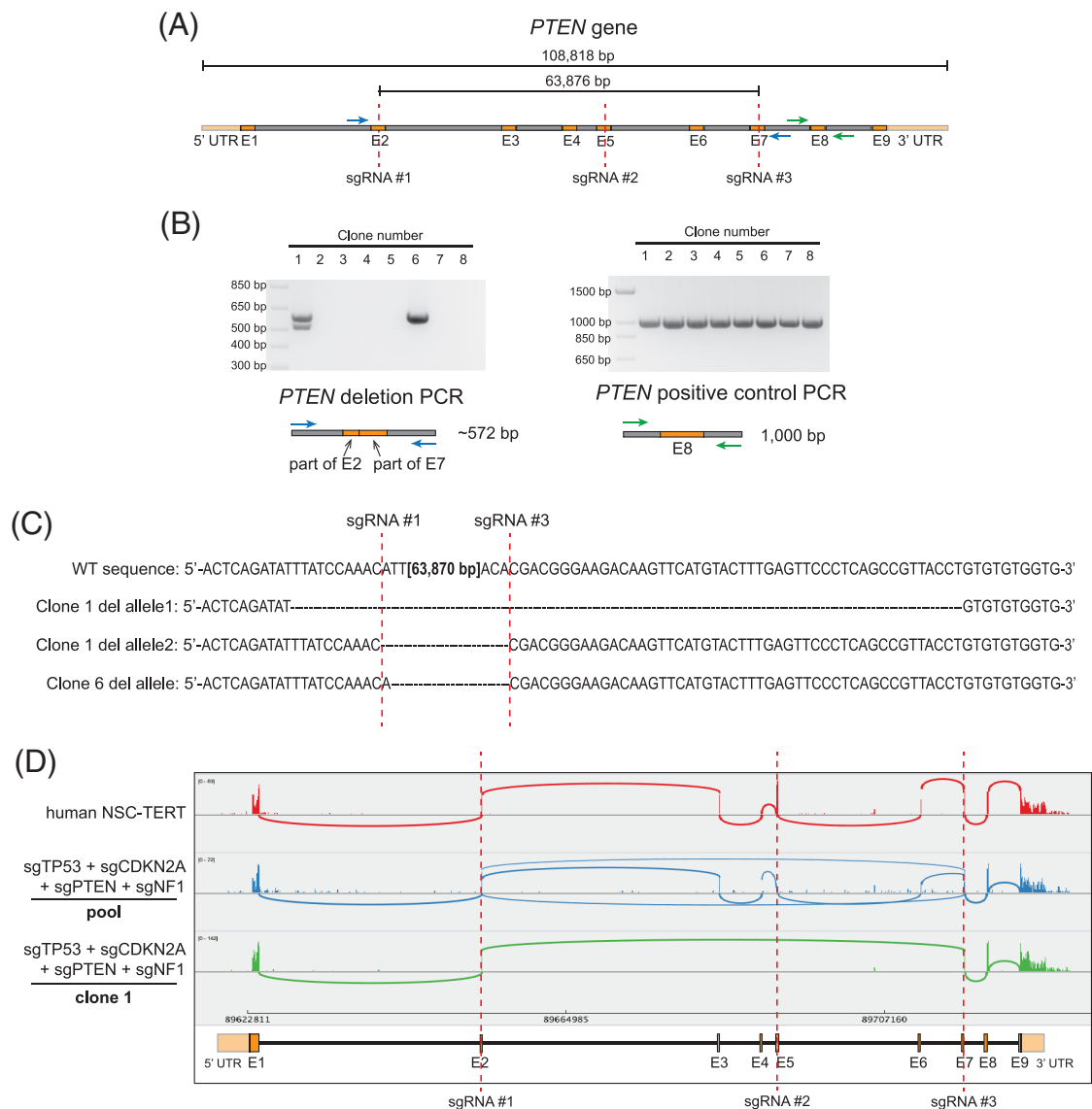


**FIGURE 4** Cas9:sgRNA RNPs can be used to generate large genomic deletions in cell clones. A, The targeting strategy for the *PTEN* gene. Three sgRNAs were designed targeting exons 2, 5, and 7. To check for the potential deletion of the ~64 kb segment between the outermost sgRNAs, deletion PCR primers (in blue) were devised to amplify a product only if the entire region had been deleted. Amplification of the region around the non-targeted exon 8 (primers in green) served as a positive control for gDNA integrity. (B) Left: Deletion PCR as described in A for 8 different clones of transformed NSC-CB660 that had been nucleofected with the 3 sgRNAs targeting *PTEN*. Right: Positive control PCR as described in A for the 8 clones. C, Genomic sequences of the 3 deletion alleles identified in B. Red dotted lines denote sgRNA cut sites. D, A sashimi plot of RNA-seq reads covering the *PTEN* gene for parental NSC cells, targeted pool, and clone 1. "Transcripts" with a minimum junction coverage of 5 reads are shown

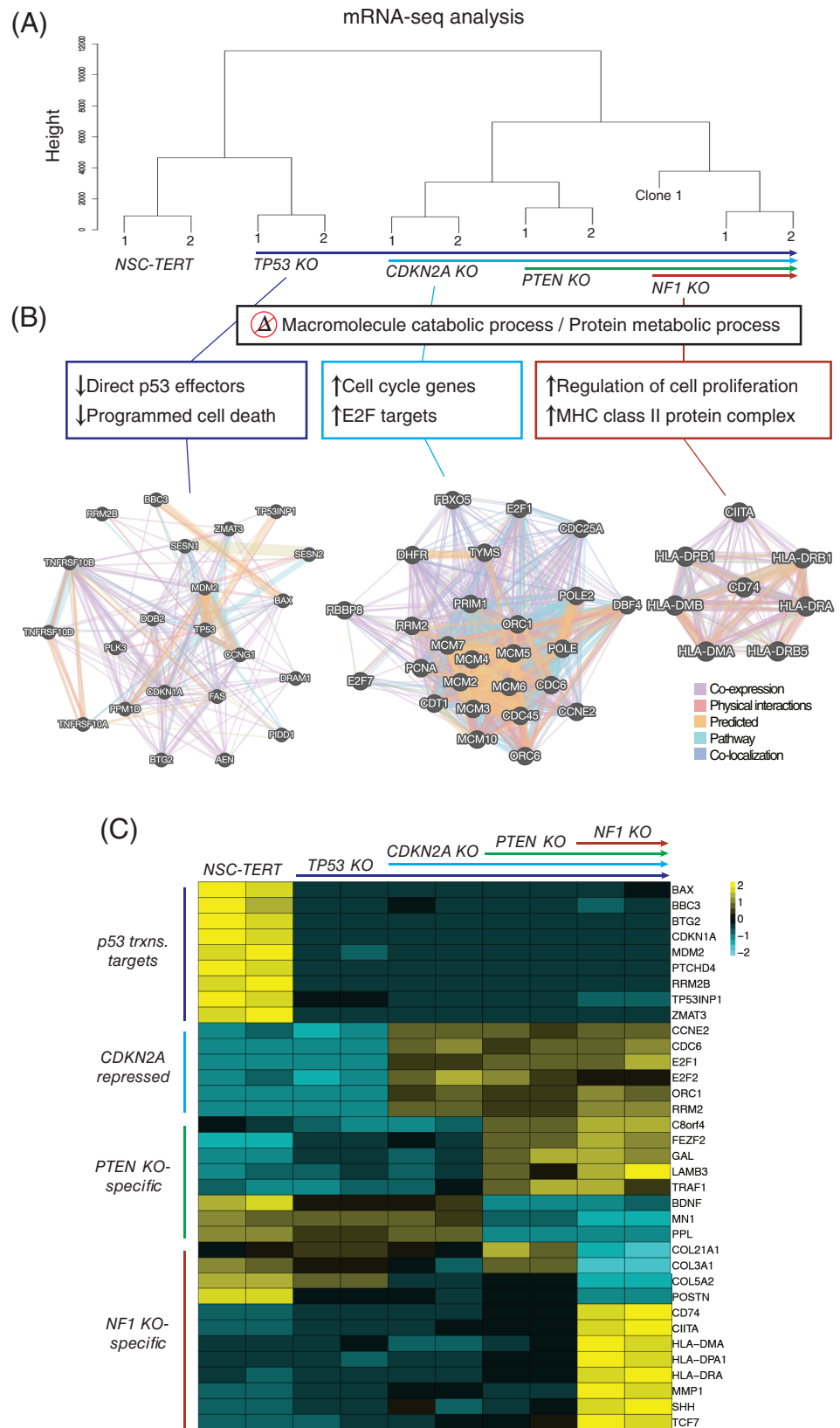
*PLK1* interactions (50 genes,  $P = 6.4E-20$ ). Thus, loss of *CDKN2A* leads to profound reprogramming of the transcription of critical cell cycle-regulated genes in human NSCs, consistent with loss of p16 function.

In contrast to *TP53* and *CDKN2A*, *PTEN* KO produced the fewest changes in gene expression in our scheme (upregulation of 169 genes and downregulation of 216 genes [ $\pm 0.5 \log_2FC$ ,  $FDR < 0.05$ ]). This may be due to epistasis with gene expression changes caused by *CDKN2A* KO. Nonetheless, manual curation of these genes revealed possible connections to the PI-3 kinase pathway itself, suggestive of feedback regulation. For example, within the downregulated genes,

*PPL/Plakin* binds AKT directly,<sup>42</sup> and brain-derived neurotrophic factor (BDNF) activates AKT<sup>43</sup> and *PTEN* itself.<sup>44</sup> Within the upregulated genes, *GAL/galanin* codes for a neuroendocrine peptide that exhibits an autocrine mitogenic effect through ERK and AKT activity<sup>45</sup> (Figure 5C). In addition, there were many novel genes affected by *PTEN* loss, including: *C8orf4/TCIM*, a positive regulator of the Wnt/beta-catenin pathway<sup>45</sup>; *FEZF2*, a marker and transcription factor associated with NSC-dependent patterning of the cerebral cortex<sup>46</sup>; and *TRAF1*, which mediates the anti-apoptotic signals from TNF receptors<sup>47</sup> (Figure 5C).



**FIGURE 5** Gene expression changes induced by tumor suppressor knockout targeting events in human NSCs. A, Cluster analysis showing relative gene expression profile relationships based on RNA-seq for parental NSC-TERT cells and NSC-TERT successively nucleofected with sgTP53s, then sgCDKN2As, then sgPTENs, and then sgNF1s, as well as for clone 1 derived from the final pool where all 4 genes had been targeted. Duplicates were sequenced for all samples except clone 1. B, Networks showing gene relationships for genes altered upon TP53, CDKN2A, or NF1 knockout. C, Heatmap displaying examples of sgTP53, sgCDKN2A, sgPTEN, and sgNF1-specific gene expression changes observed in RNA-seq data. Relative gene expression values were normalized for all samples within each gene. Each RNA-seq replicate is shown as a separate column



With the further addition of *NF1* KO in *TP53* + *CDKN2A* + *PTEN* KO cells, we observed changes in expression of an additional 1022 genes (321 up- and 701 downregulated;  $\log_2FC \pm 0.5$ ;  $FDR < 0.05$ ).

The downregulated genes were most significantly enriched for extracellular matrix organization genes (43 genes, GO:0030198,  $P = 1.8E-15$ ), which included many collagen encoding genes and periostin

(Figure 5C). Upregulated genes included genes involved in regulation of cell proliferation (43 genes,  $P = 5.2E-6$ ), including members of the WNT signaling pathway (*WNT7B*, *FZD4*, *LEF1*, and *TCF7*). Interestingly, also upregulated were eight genes coding for major histocompatibility complex (MHC) class II proteins, including *CIITA*, the master transcriptional activator controlling expression of the MHC class II genes<sup>48</sup> (Figure 5B,C; Tables S2 and S3). *CIITA* expression was upregulated ~10-fold in *NF1* KO cells relative to NSC-TERT cells. MHC class II genes are primarily expressed by professional antigen presenting cells, such as dendritic cells, macrophages, and B cells.<sup>49</sup> However, remarkably, upregulation of MHC class II protein complex is a hallmark of *NF1*<sup>-/-</sup> human neurofibroma tumor cells, which *CIITA* activity is required to maintain.<sup>48,50</sup> It has also been observed that gliomas and other cancers have a high proportion of MHC class II-expressing tumor cells,<sup>51</sup> which may promote tolerance to tumor-associated antigens.<sup>52</sup> Our results show that *NF1* loss is one route to de-repression of MHC class II machinery in human NSCs.

In addition to gene expression changes in response to loss of *TP53*, *CDKN2A*, *PTEN*, and *NF1*, we also identified 806 genes whose expression remained largely unaltered in all conditions ( $FDR \geq 0.2$  across all comparisons with  $\geq 10$  CPM counts across all samples). Gene set enrichment analysis revealed that 487 of these were involved in a "cellular metabolic process" (GO:0044237,  $FDR = 1.5E-15$ ), with 129 encoding mitochondrial proteins (including 19 involved in oxidative phosphorylation) and 29 encoding ribosomal proteins (Tables S2 and S3). Our previous CRISPR-Cas9 lethality screens in NSC-CB660 cells demonstrate that at least 208 of these genes score as essential, including, for example, 34 genes associated with ribosome biogenesis, 11 genes coding for respiratory electron transport machinery, and 23 overlapping with "housekeeping" genes<sup>53</sup> (GSEA: 111197,  $P = 7.12E-13$ ). These results suggest that a subset of genes expressed in human NSCs are transcriptionally regulated and/or maintain their mRNA levels independently of p53, the Rb-axis, PI-3 kinase, and NF1 pathways.

Altogether, our gene expression results highlight the utility of our CRISPR-Cas9 RNP nucleofection method for quickly creating a series of KOs that allow for the study of gene activities, such as genes involved in tumor initiation. Importantly, due to the high targeting efficiency using our method, we were able to confirm many known as well as identify novel transcriptional changes associated with loss of the genes we targeted, using nucleofected cell pools rather than cell clones.

## 3 | METHODS

### 3.1 | CRISPR sgRNA design

CRISPR sgRNAs were designed via manual curation of all possible sgRNA sequences for a given region as identified by the Broad Institute's GPP Web Portal.<sup>30</sup> (See <https://portals.broadinstitute.org/gpp/public/analysis-tools/sgrna-design-help#output> for an explanation of the Broad GPP Web Portal outputs.) sgRNAs were chosen to have

high on-target efficacy scores but minimal predicted off-target effects. sgRNA sequences that had perfect matches in any other regions of the genome (ie, sgRNAs with any "Bin I" matches) were NOT chosen. sgRNAs with the lowest possible number of "Bin II" off-target matches were chosen, particularly the lowest possible number of "Bin II, Tier I and Tier II" matches. See Table S1 for a list of all sgRNA sequences used.

### 3.2 | Cas9:sgRNA RNP nucleofection

See detailed protocol in Data S1. Briefly, to prepare RNP complexes, reconstituted sgRNA (Synthego) and then sNLS-SpCas9-sNLS (Aldevron) were added to complete SG Cell Line Nucleofector Solution (Lonza), to a final volume of 20  $\mu$ L. The mixture was incubated at room temperature for 15 minutes to allow RNP complexes to form. A Cas9:sgRNA molar ratio of 1:2 was used, unless otherwise noted. Total RNP doses described refer to the amount of the limiting complex member (Cas9). To nucleofect,  $1.5 \times 10^5$  cells were harvested, washed with PBS, resuspended in 20  $\mu$ L of RNPs, and electroporated using the Amaxa 96-well Shuttle System or 4D X Unit (Lonza) and program EN-138.

### 3.3 | CRISPR editing analysis

Nucleofected cells were harvested at indicated timepoints and genomic DNA was extracted (MicroElute Genomic DNA Kit, Omega Bio-Tek). Genomic regions around CRISPR target sites were PCR amplified using Phusion polymerase (Thermo Fisher Scientific) and primers located (whenever possible) at least 250 bp outside sgRNA cut sites. After size verification by agarose gel electrophoresis, PCR products were column-purified (Monarch PCR & DNA Clean-up Kit, New England BioLabs) and submitted for Sanger sequencing (Genewiz) using unique sequencing primers. The resulting trace files for edited cells vs control cells (nucleofected with non-targeting Cas9:sgRNA RNPs) were analyzed for predicted indel composition using the Inference of CRISPR Edits (ICE) web tool.<sup>28</sup> See detailed CRISPR RNP nucleofection protocol in Data S1 for general PCR conditions used for Phusion polymerase. See Table S1 for a list of all PCR and sequencing primers used, as well as PCR conditions specific to particular genomic regions.

### 3.4 | Cell culture

Patient tumor-derived GSCs and fetal tissue-derived NSCs were provided by Drs. Do-Hyun Nam, Jeongwu Lee, and Steven M. Pollard, were obtained via informed consent, and have been previously published.<sup>54-56</sup> Isolates were cultured in NeuroCult NS-A basal medium (StemCell Technologies) supplemented with B27 (Thermo Fisher Scientific), N2 (homemade 2x stock in Advanced DMEM/F-12 (Thermo Fisher Scientific)), EGF and FGF-2 (20 ng/mL) (PeproTech), glutamax

(Thermo Fisher Scientific), and antibiotic-antimycotic (Thermo Fisher Scientific). Cells were cultured on laminin (Trevigen or in-house-purified) -coated polystyrene plates and passaged as previously described,<sup>54</sup> using Accutase (EMD Millipore) to detach cells.

### 3.5 | Western blotting

Cells were harvested, washed with PBS, and lysed with modified RIPA buffer (150 mM NaCl, 25 mM Tris-HCl (pH 8.0), 1 mM EDTA, 1.0% Igepal CA-630 (NP-40), 0.5% sodium deoxycholate, 0.1% SDS, 1X protease inhibitor cocktail (complete Mini EDTA-free, Roche)). Lysates were sonicated (Bioruptor, Diagenode) and then quantified using Pierce BCA assay (Thermo Fisher Scientific). Identical amounts of proteins (20–40  $\mu$ g) were electrophoresed on 4% to 15% Mini-PROTEAN TGX precast protein gels (Bio-Rad). For transfer, the Trans-Blot Turbo transfer system (Bio-Rad) with nitrocellulose membranes was used according to the manufacturer's instructions. TBS (137 mM NaCl, 20 mM Tris, pH 7.6) +5% nonfat milk was used for blocking, and TBS + 0.1% Tween-20 + 5% milk was used for antibody incubations. The following commercial primary antibodies were used: Tp53 (Cell Signaling #48818, 1:500), p14/ARF (Bethyl Laboratories #A300-340A-T, 1:500), p16/INK4A (Abcam #ab16123, 1:200), PTEN (Cell Signaling #9559S, 1:1000), NF1 (Santa Cruz #sc-67, 1:50),  $\alpha$ Tubulin (Sigma #T9026, 1:1000), GAPDH (Sigma #SAB2500450, 1:100). The following secondary antibodies were used (LI-COR): #926-68 073, #926-32 212, #926-32 214, #926-68 074. An Odyssey infrared imaging system (LI-COR) was used to visualize blots.

### 3.6 | RNA-seq and analysis

Cells were lysed with Trizol (Thermo Fisher Scientific). Total RNA was isolated (Direct-zol RNA kit, Zymo Research) and quality validated on the Agilent 2200 TapeStation. Illumina sequencing libraries were generated with the KAPA Biosystems Stranded RNA-Seq Kit<sup>57</sup> and sequenced using HiSeq 2000 (Illumina) with 100 bp paired-end reads (~11.3–13.8 million paired reads per replicate). RNA-seq reads were aligned to the UCSC hg19 assembly using STAR2 (v 2.6.1)<sup>58</sup> (~82.0%–88.5% of reads uniquely aligned to the genome for each replicate) and counted for gene associations against the UCSC genes database with HTSeq.<sup>59</sup> Normalized gene count data was used for subsequent hierarchical clustering (R package ggplot2<sup>60</sup>) and differential gene expression analysis (R/Bioconductor package edgeR<sup>39</sup>). Heatmaps were made using R package pheatmap.<sup>61</sup>

## 4 | DISCUSSION

Here, we present a method for creating bi- and multi-allelic loss-of-function indel mutations, using in vitro assembled Cas9:sgRNA RNPs composed of chemically synthesized, modified sgRNA and purified Cas9 protein. By this method, indel efficiencies >90% can routinely be

achieved in populations of cells, obviating the need for clonal selection of edited cells or chemical selection of DNA-based sgRNA expression systems. We demonstrate that even in cell pools, this approach leads to near-total protein loss and can be easily used to study the consequences of various gene knockouts, such as the effects of loss of tumor suppressors on oncogenic transformation of normal cells. Moreover, because gene editing is complete within 3 days of RNP introduction, this approach offers better experimental tractability over current approaches, which can suffer from lack of indel penetrance and protracted windows of indel formation.

This method also improves upon existing methods for the creation of precise or near-precise deletions. In mammals, single dsDNA breaks, including those generated by Cas9:sgRNA cutting, produce NHEJ-dependent small insertions or deletions at break sites (ie, error-prone repair).<sup>11,62</sup> However, adding a second dsDNA break in close proximity to the first can cause rejoining without error via "accurate" NHEJ.<sup>63,64</sup> Our results support this notion. We observe a high frequency and penetrance of conversion of single indels to precise and near-precise deletions. It has been previously shown that using 2 to 3 proximal sgRNAs can create deletions of ~10 bp to 1 Mbp in mouse embryos and cultured cells.<sup>4,63,65,66</sup> However, these approaches produce deletion formation efficiencies ranging from ~2% to ~40%. By contrast, using our method we observe near-precise deletion frequencies as high as >90% using sgRNAs spaced up to 1000 bp apart. In addition, we observe that larger deletions are also possible, as in the case of our targeting of *PTEN*, where 25% of clones contained a ~64 kbp deletion in at least one allele. Our results suggest that the use of 2 to 3 sgRNAs with our approach can have the added benefit of triggering accurate NHEJ and being able to specify a high frequency of precise or near-precise deletions. The deletion efficiency decreases as the size of the desired deletion increases, meaning that single-cell clones may need to be created to study larger deletions. However, since the efficiencies obtained using our method are significantly higher than with other methods, fewer clones need to be expanded and evaluated, saving time and resources.

This technique does have a few limitations. First, achieving high multi-allelic indel efficiencies may require pre-validation of sgRNAs. However, we have had good success designing sgRNAs using the Broad GPP Web Portal design tool (where ~60%–70% of sgRNAs that we choose via manual curation produce >80% indel formation) or, alternatively, choosing sgRNA sequences from positively scoring CRISPR-Cas9 lentiviral-based screen hits. Second, reliance on chemically synthesized sgRNAs can be cost-prohibitive for large-scale projects. An alternative option is to generate in vitro transcribed sgRNA using T7, T3, or SP6 RNA polymerase in the presence of ribonucleoside triphosphates and a DNA template.<sup>3</sup> However, this requires additional steps, namely the initial creation of an accurate DNA template and the purification of the transcribed sgRNA to remove unincorporated triphosphates, enzyme, and template DNA. In addition, in vitro transcription can result in errors toward the 5' end of the RNA.<sup>67</sup> Also, it is not possible to easily generate modifications, meaning in vitro transcribed sgRNAs do not possess increased protection from nucleases once they have entered the cell, resulting in decreased

editing efficiency compared to chemically synthesized, modified sgRNAs. Nonetheless, this is a viable alternative to consider when cost is a concern. Another alternative is to employ a commercially sourced dual gRNA system (crRNA:tracrRNA), which may represent only a slight reduction in efficiency. The two chemically synthesized RNAs can still be modified to enhance nuclease resistance, but they are usually available at a lower cost since the accurate synthesis of these shorter RNAs is less complex compared to a longer chimeric sgRNA.

Our data suggest that the relatively simple method described here can be used for highly efficient (>90%) and fast (72 hours) gene knockout, as well as for targeted genomic deletions, even in hyperdiploid cells (such as many tumor cells). This represents an extremely useful tool for inactivating not only coding genes, but also non-coding elements such as non-coding RNAs, UTRs, enhancers, and promoters. The gain in efficiency that we observe can allow for systematic well-by-well screening (similar to small interfering RNA screens), but provides the flexibility of targeting any small element in the genome. This method can be readily applied to diverse mammalian cell types by varying the nucleofection buffer and program. (Lonza can provide appropriate conditions for many cell types.) Thus, it represents an important step forward in the ability to manipulate the genomes of cell cultures derived from primary cells, such as patient-derived tumor cells and human stem/progenitor cells.

#### ACKNOWLEDGEMENTS

We thank members of the Paddison laboratory for helpful discussions and critical reading of the manuscript; Do-Hyun Nam, Jeongwu Lee, and Steven M. Pollard for providing cell isolates; Franziska Michor for helpful suggestions; David McDonald in the Cellular Imaging Core for performing karyotyping analysis; and Pam Lindberg and An Tyrrell for administrative support. *Funding Sources:* National Institutes of Health (T32 CA080416 to P.H., R01 CA190957, P30 DK56465-13, U54 DK106829, P30 CA015704); American Cancer Society (ACS-RSG-14-056-01); Robert J. Kleberg, Jr. and Helen C. Kleberg Foundation.

#### CONFLICT OF INTEREST

The authors declare no potential conflict of interest.

#### AUTHORS' CONTRIBUTIONS

*Conceptualization*, Pia Hoellerbauer, Hua-Jun Wu, and Patrick J. Paddison; *Methodology*, Pia Hoellerbauer, Megan Kufeld, and Patrick J. Paddison; *Validation*, Pia Hoellerbauer and Megan Kufeld; *Investigation*, Pia Hoellerbauer, Megan Kufeld, and Heather M. Feldman; *Formal Analysis*, Pia Hoellerbauer, Megan Kufeld, and Sonali Arora; *Writing - Original Draft*, Pia Hoellerbauer and Patrick J. Paddison; *Writing - Review & Editing*, Pia Hoellerbauer, Megan Kufeld, and Patrick J. Paddison; *Visualization*, Pia Hoellerbauer, Sonali Arora, and Patrick J. Paddison; *Supervision*, Patrick J. Paddison; *Funding Acquisition*, Patrick J. Paddison. All authors read and approved the final manuscript.

#### ETHICAL STATEMENT

We followed the guidelines set by the Fred Hutchinson Cancer Research Center Institutional Review Office for De-identified Human Specimens and/or Data, which categorizes the studies presented here as Research Not Involving Human Subjects as detailed by the Institutional Review Board's Human Subjects Research Determination Form.

#### DATA AVAILABILITY STATEMENT

The data that supports the findings of this study are available in the supplementary material of this article. The RNA-seq data that support the findings of this study are openly available in the NCBI Gene Expression Omnibus at <https://www.ncbi.nlm.nih.gov/geo/>, GEO accession number GSE149485.

#### ORCID

Patrick J. Paddison  <https://orcid.org/0000-0002-7144-0228>

#### REFERENCES

- Wiedenheft B, Sternberg SH, Doudna JA. RNA-guided genetic silencing systems in bacteria and archaea. *Nature*. 2012;482(7385):331-338.
- Mali P, Esvelt KM, Church GM. Cas9 as a versatile tool for engineering biology. *Nat Methods*. 2013;10(10):957-963.
- Cho SW, Kim S, Kim JM, Kim JS. Targeted genome engineering in human cells with the Cas9 RNA-guided endonuclease. *Nat Biotechnol*. 2013;31(3):230-232.
- Cong L, Ran FA, Cox D, et al. Multiplex genome engineering using CRISPR/Cas systems. *Science*. 2013;339:819-823.
- Jinek M, East A, Cheng A, Lin S, Ma E, Doudna J. RNA-programmed genome editing in human cells. *Elife*. 2013;2:e00471.
- Mali P, Yang L, Esvelt KM, et al. RNA-guided human genome engineering via Cas9. *Science*. 2013;339:823-826.
- Jinek M, Chylinski K, Fonfara I, Hauer M, Doudna JA, Charpentier E. A programmable dual-RNA-guided DNA endonuclease in adaptive bacterial immunity. *Science*. 2012;337:816-821.
- Ran FA, Hsu PD, Wright J, Agarwala V, Scott DA, Zhang F. Genome engineering using the CRISPR-Cas9 system. *Nat Protoc*. 2013;8:2281-2308.
- Hartlerode AJ, Scully R. Mechanisms of double-strand break repair in somatic mammalian cells. *Biochem J*. 2009;423(2):157-168.
- Lieber MR, Ma Y, Pannicke U, Schwarz K. Mechanism and regulation of human non-homologous DNA end-joining. *Nat Rev Mol Cell Biol*. 2003;4(9):712-720.
- Chakrabarti AM, Henser-Brownhill T, Monserrat J, Poetsch AR, Luscombe NM, Scaffidi P. Target-specific precision of CRISPR-mediated genome editing. *Mol Cell*. 2019;73(4):699-713 e6.
- Shalem O, Sanjana NE, Hartenian E, et al. Genome-scale CRISPR-Cas9 knockout screening in human cells. *Science*. 2014;343:84-87.
- Wang T, Wei JJ, Sabatini DM, Lander ES. Genetic screens in human cells using the CRISPR-Cas9 system. *Science*. 2014;343:80-84.
- Toledo CM, Ding Y, Hoellerbauer P, et al. Genome-wide CRISPR-Cas9 screens reveal loss of redundancy between PKMYT1 and WEE1 in Glioblastoma stem-like cells. *Cell Rep*. 2015;13(11):2425-2439.
- Liang X, Potter J, Kumar S, et al. Rapid and highly efficient mammalian cell engineering via Cas9 protein transfection. *J Biotechnol*. 2015;208:44-53.
- Kim S, Kim D, Cho SW, Kim J, Kim JS. Highly efficient RNA-guided genome editing in human cells via delivery of purified Cas9 ribonucleoproteins. *Genome Res*. 2014;24(6):1012-1019.

17. Zuris JA, Thompson DB, Shu Y, et al. Cationic lipid-mediated delivery of proteins enables efficient protein-based genome editing in vitro and in vivo. *Nat Biotechnol.* 2014;33:73.
18. DeWitt MA, Corn JE, Carroll D. Genome editing via delivery of Cas9 ribonucleoprotein. *Methods.* 2017;121-122:9-15.
19. Schumann K, Lin S, Boyer E, et al. Generation of knock-in primary human T cells using Cas9 ribonucleoproteins. *Proc Natl Acad Sci.* 2015;112(33):10437-10442.
20. Lin S, Staahl BT, Alla RK, Doudna JA. Enhanced homology-directed human genome engineering by controlled timing of CRISPR/Cas9 delivery. *Elife.* 2014;3:e04766.
21. Bressan RB, Dewari PS, Kalantzi M, et al. Efficient CRISPR/Cas9-assisted gene targeting enables rapid and precise genetic manipulation of mammalian neural stem cells. *Development.* 2017;144:635-648.
22. Graf R, Li X, Chu VT, Rajewsky K. sgRNA sequence motifs blocking efficient CRISPR/Cas9-mediated gene editing. *Cell Rep.* 2019;26(5):1098-103.e3.
23. Eckstein F. Phosphorothioates, essential components of therapeutic oligonucleotides. *Nucleic Acid Ther.* 2014;24(6):374-387.
24. Allerson CR, Sioufi N, Jarres R, et al. Fully 2'-modified oligonucleotide duplexes with improved in vitro potency and stability compared to unmodified small interfering RNA. *J Med Chem.* 2005;48(4):901-904.
25. Hendel A, Bak RO, Clark JT, et al. Chemically modified guide RNAs enhance CRISPR-Cas genome editing in human primary cells. *Nat Biotechnol.* 2015;33(9):985-989.
26. Choung S, Kim YJ, Kim S, Park H-O, Choi Y-C. Chemical modification of siRNAs to improve serum stability without loss of efficacy. *Biochem Biophys Res Commun.* 2006;342(3):919-927.
27. Brinkman EK, Chen T, Amendola M, van Steensel B. Easy quantitative assessment of genome editing by sequence trace decomposition. *Nucleic Acids Res.* 2014;42(22):e168.
28. Hsiao T, Conant D, Maures T, Waite K, Yang J, Kelso R, et al. Inference of CRISPR Edits from Sanger Trace Data. bioRxiv. 2019.
29. Vakulskas CA, Behlke MA. Evaluation and reduction of CRISPR off-target cleavage events. *Nucleic Acid Ther.* 2019;29(4):167-174.
30. Doench JG, Fusi N, Sullender M, et al. Optimized sgRNA design to maximize activity and minimize off-target effects of CRISPR-Cas9. *Nat Biotechnol.* 2016;34(2):184-191.
31. Ozawa T, Riestler M, Cheng YK, et al. Most human non-GCIMP Glioblastoma subtypes evolve from a common proneural-like precursor Glioma. *Cancer Cell.* 2014;26(2):288-300.
32. Alcantara Llaguno S, Chen J, Kwon C-H, et al. Malignant Astrocytomas originate from neural stem/progenitor cells in a somatic tumor suppressor mouse model. *Cancer Cell.* 2009;15(1):45-56.
33. Kwon C-H, Zhao D, Chen J, et al. Pten Haploinsufficiency accelerates formation of high-grade Astrocytomas. *Cancer Res.* 2008;68(9):3286-3294.
34. Llaguno SA, Chen J, Kwon CH, Parada LF. Neural and cancer stem cells in tumor suppressor mouse models of malignant astrocytoma. *Cold Spring Harb Symp Quant Biol.* 2008;73:421-426.
35. Zheng H, Ying H, Yan H, et al. p53 and Pten control neural and glioma stem/progenitor cell renewal and differentiation. *Nature.* 2008;455(7216):1129-1133.
36. Zhu Y, Guignard F, Zhao D, et al. Early inactivation of p53 tumor suppressor gene cooperating with NF1 loss induces malignant astrocytoma. *Cancer Cell.* 2005;8(2):119-130.
37. Marumoto T, Tashiro A, Friedmann-Morvinski D, et al. Development of a novel mouse glioma model using lentiviral vectors. *Nat Med.* 2009;15(1):110-116.
38. Brennan CW, Verhaak RGW, McKenna A, et al. The somatic genomic landscape of glioblastoma. *Cell.* 2013;155:462-477.
39. Robinson MD, McCarthy DJ, Smyth GK. edgeR: a bioconductor package for differential expression analysis of digital gene expression data. *Bioinformatics.* 2010;26(1):139-140.
40. Fischer M. Census and evaluation of p53 target genes. *Oncogene.* 2017;36(28):3943-3956.
41. Sherr CJ, McCormick F. The RB and p53 pathways in cancer. *Cancer Cell.* 2002;2(2):103-112.
42. van den Heuvel AP, de Vries-Smits AM, van Weeren PC, et al. Binding of protein kinase B to the plakin family member periplakin. *J Cell Sci.* 2002;115(Pt 20):3957-3966.
43. Song W, Volosin M, Cragnolini AB, Hempstead BL, Friedman WJ. ProNGF induces PTEN via p75NTR to suppress Trk-mediated survival signaling in brain neurons. *J Neurosci.* 2010;30(46):15608-15.
44. Plotkin JL, Day M, Peterson JD, et al. Impaired TrkB receptor signaling underlies corticostriatal dysfunction in Huntington's disease. *Neuron.* 2014;83(1):178-188.
45. Banerjee R, Henson BS, Russo N, Tsodikov A, D'Silva NJ. Rap1 mediates galanin receptor 2-induced proliferation and survival in squamous cell carcinoma. *Cell Signal.* 2011;23(7):1110-1118.
46. Dwyer ND, Chen B, Chou SJ, Hippenmeyer S, Nguyen L, Ghashghaei HT. Neural stem cells to cerebral cortex: emerging mechanisms regulating progenitor behavior and productivity. *J Neurosci.* 2016;36(45):11394-401.
47. Shu HB, Takeuchi M, Goeddel DV. The tumor necrosis factor receptor 2 signal transducers TRAF2 and c-IAP1 are components of the tumor necrosis factor receptor 1 signaling complex. *Proc Natl Acad Sci U S A.* 1996;93(24):13973-8.
48. Choi NM, Majumder P, Boss JM. Regulation of major histocompatibility complex class II genes. *Curr Opin Immunol.* 2011;23(1):81-87.
49. Neeffjes J, Jongsma ML, Paul P, Bakke O. Towards a systems understanding of MHC class I and MHC class II antigen presentation. *Nat Rev Immunol.* 2011;11(12):823-836.
50. Reuss DE, Mucha J, Holtkamp N, et al. Functional MHC class II is upregulated in neurofibromin-deficient Schwann cells. *J Invest Dermatol.* 2013;133(5):1372-1375.
51. Tran CT, Wolz P, Egensperger R, et al. Differential expression of MHC class II molecules by microglia and neoplastic astroglia: relevance for the escape of astrocytoma cells from immune surveillance. *Neuropathol Appl Neurobiol.* 1998;24(4):293-301.
52. Thibodeau J, Bourgeois-Daigneault MC, Lapointe R. Targeting the MHC class II antigen presentation pathway in cancer immunotherapy. *Oncotargets Ther.* 2012;1(6):908-916.
53. Hsiao LL, Dangond F, Yoshida T, et al. A compendium of gene expression in normal human tissues. *Physiol Genomics.* 2001;7(2):97-104.
54. Pollard SM, Yoshikawa K, Clarke ID, et al. Glioma stem cell lines expanded in adherent culture have tumor-specific phenotypes and are suitable for chemical and genetic screens. *Cell Stem Cell.* 2009;4:568-580.
55. Sun Y, Pollard S, Conti L, et al. Long-term tripotent differentiation capacity of human neural stem (NS) cells in adherent culture. *Mol Cell Neurosci.* 2008;38:245-258.
56. Lee J, Kotliarova S, Kotliarov Y, et al. Tumor stem cells derived from glioblastomas cultured in bFGF and EGF more closely mirror the phenotype and genotype of primary tumors than do serum-cultured cell lines. *Cancer Cell.* 2006;9:391-403.
57. Hart T, Chandrasekhar M, Aregger M, et al. High-resolution CRISPR screens reveal fitness genes and genotype-specific cancer liabilities. *Cell.* 2015;163(6):1515-1526.
58. Dobin A, Davis CA, Schlesinger F, et al. STAR: ultrafast universal RNA-seq aligner. *Bioinformatics.* 2013;29(1):15-21.
59. Anders S, Pyl PT, Huber W. HTSeq—a python framework to work with high-throughput sequencing data. *Bioinformatics.* 2015;31(2):166-169.
60. Wickham H, Sievert C. *Ggplot2: Elegant Graphics for Data analysis.* Springer-Verlag New York; 2016.
61. Kolde R. Pheatmap: Pretty Heatmaps. R package version 1.0.10. Retrieved from <https://CRAN.R-project.org/package=pheatmap>. 2018.
62. Symington LS, Gautier J. Double-strand break end resection and repair pathway choice. *Annu Rev Genet.* 2011;45:247-271.

63. Guo T, Feng YL, Xiao JJ, et al. Harnessing accurate non-homologous end joining for efficient precise deletion in CRISPR/Cas9-mediated genome editing. *Genome Biol.* 2018;19(1):170.
64. Betermier M, Bertrand P, Lopez BS. Is non-homologous end-joining really an inherently error-prone process? *PLoS Genet.* 2014;10(1):e1004086.
65. Canver MC, Bauer DE, Dass A, et al. Characterization of genomic deletion efficiency mediated by clustered regularly interspaced short palindromic repeats (CRISPR)/Cas9 nuclease system in mammalian cells. *J Biol Chem.* 2014;289(31):21312–24.
66. Wolfs JM, Hamilton TA, Lant JT, et al. Biasing genome-editing events toward precise length deletions with an RNA-guided TevCas9 dual nuclease. *Proc Natl Acad Sci U S A.* 2016;113(52):14988–93.
67. Helm M, Brulé H, Giegé R, Florentz C. More mistakes by T7 RNA polymerase at the 5' ends of in vitro-transcribed RNAs. *RNA.* 1999;5:618–621.

## SUPPORTING INFORMATION

Additional supporting information may be found online in the Supporting Information section at the end of this article.

**How to cite this article:** Hoellerbauer P, Kufeld M, Arora S, Wu H-J, Feldman HM, Paddison PJ. A simple and highly efficient method for multi-allelic CRISPR-Cas9 editing in primary cell cultures. *Cancer Reports.* 2020;3:e1269. <https://doi.org/10.1002/cnr2.1269>